Supporting Information

Dynamic self-assemby of detonation nanodiamond in water

Shery L.Y. Chang

Eyring Materials Center and School of Molecular Sciences, Arizona State University, Tempe, USA

Philipp Reineck

ARC Centre of Excellence for Nanoscale BioPhotonics, School of Science, RMIT University, Melbourne, Australia.

Dewight Williams

Eyring Materials Center, Arizona State University, Tempe, USA

Gary Bryant

School of Science, RMIT University, Melbourne, Australia.

George Opletal and Amanda S. Barnard

Data61, CSIRO, Docklands, Australia

Samir A. El-Demrdash

School of Science, RMIT University, Melbourne, Australia..

Po-Lin Chiu

School of Molecular Sciences, Arizona State University, Tempe, USA

Eiji Ōsawa

NanoCarbon Research Institute, Ueda, Japan

Christian Dwyer

Department of Physics, Arizona State University, Tempe, USA

A. Synthesis of dispersed detonation nanodiamond (DND) with different surface chemistry

The DND presented in the main text is rich in C-H group. It is provided by NanoCarbon Research Institute. The details of the synthesis can be found in Ref [1] and a short description is as follows:

Commercial crude products of detonation nanodiamond were purchased from Comstar Technology Limited, Hong Kong. This material is composed of large and extremely tight agglutinates of the elementary particles of DND, and disintegrated by means of attrition milling. The milling and work-up consist of (1) suspending the as-received agglutinates in water by high-speed agitation using a T.K.Robomix (model f, Primix Co., Tokyo); (2) circulating the suspension through a vertical attrition mill equipped with centrifugal separator and connected in series with a 450W vertically vibrating sonication rod to give a black aqueous solution of crude elementary particle of DND; (3) the solution is then subjected to refrigerating to separate uncrushed solid contaminants; (4) final centrifugal separation to remove metal oxides and other heavy impurities as precipitates; (5) the slightly viscous aqueous solution is collected by decantation to give dispersed colloidal elementary particles of DND in water. The sizes were measured to be 4.1± 0.5 nm and the ζ-potential >+50 mV.

The DND with surface groups rich in -COOH is provided by Adamas Nanotechnologies, Inc.. The details of the synthesis of this DND can be found in Ref [2]. The short description is given below:

DND were produced via detonation of an oxygen-deficient explosive mixtures of trinitrotoluene with hexogen (50:50 wt.%) in a closed steel chamber using CO_2 cooling media. The detonation soot product is a mixture of up to 30 wt% of diamond particulates in addition to other carbon allotropes and metallic impurities. This product was subsequently purified by oxidation of the soot in a mixture of nitric and sulfuric acid in the presence of sulfur oleate at high temperature (above 200°C). The residual content of incombustible metallic impurities in DNDs was estimated to be 1 wt%, and subsequent purification using hydrochloric acid (HCl) reduced the metal content to 0.5 wt.% as determined by Proton Induced X-Ray Emission (PIXE) analysis performed by Elemental Analysis Inc. (Lexington, Kentucky, USA). The purified raw diamond aggregates were suspended in deionized water (DI water) and processed in a planetary bead mill (Retsch GmbH) using 300 μm zirconia beads for 2 hours.

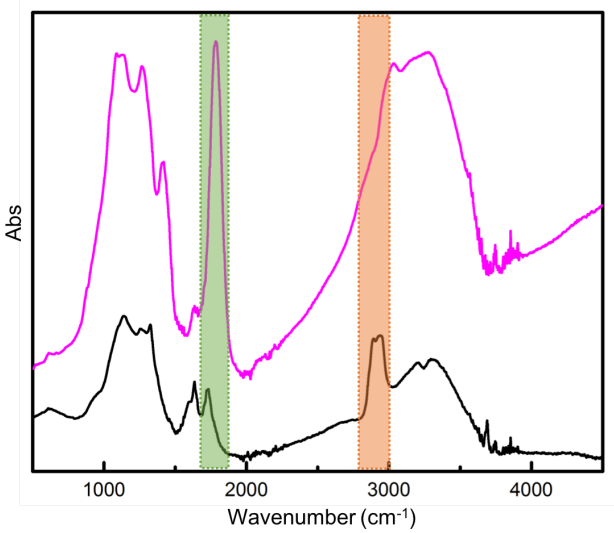

FIG. S1. FT-IR spectra of the two DNDs with different surface chemistry. The black solid line represents the DND rich in C-H, and the magenta solid line represents that rich in carboxylic group.

The milled material was then fractionated using centrifugation at 25,000 RCF for 2 hours. The zeta potential of this material is around -35 mV at a pH of 6.8 in deionized water.

The surface chemistry of these two samples were measured using FT-IR. The result is shown in Fig.S1.

B. DLS and SAXS measurements

DLS measurements were carried out using an ALV-5022F light scattering spectrometer with a laser wavelength of 633 nm and a scattering angle of 90°. DND were dispersed in deionized water at a concentration of (1 mg mL^{-1})), sufficient to ensure good scattering without any multiple scattering. All acquisition parameters can be closely controlled and the raw data is analysed using three methods using the in-built software: a cumulant analysis (which yields an average intensity weighted particle size); a distribution analysis which yields an intensity weighted size distribution; and a number weighted distribution which is a transformation of the intensity weighted distribution which assumes that all scatterers are spherical. Care needs to be taken in the interpretation of this data in cases where non-spherical scatterers may be present. SAXS measurements were carried out on a Bruker

MicroCalix small angle x-ray instrument oper ating on a Cu K_α microfocus source at wavelength 1.54 Å. SAXS data was collected on a Pilatus 100k 2D detector. The sample and background were measured in 1.5 mm diameter quartz capillaries, with exposure times of 2 hours. The data were fit using SASView 5.0 [3] using a Guinier-Porod function [4].

C. Cryo-TEM specimen preparation and imaging

Cryo-TEM specimen for the as-received DND particles in DI water with the concentration of 1 w/v % was prepared by the plunge-freezing method. Such method is well established to preserve the original state of material in the hydrated state or in the aqueous environment. This method is commonly used in the structure biology field to "fix" the biological sample in its "native" state, allowing cryo-TEM imaging without damaging the structure, due to dehydration in the vacuum environment of the TEM column. To achieve this, the DND particles in aqueous dispersion were firstly sonicated (Branson) for 15 minutes. The dispersion were then immobilized in its surrounding water by rapidly freezing (at a rate of 10^6 °C/sec) the sample so that the water in the specimen is fixed in a vitreous state. This rapid freezing prevent the formation of crystalline ice, which might result in the "distortion" of the materials native state. Preparation of the DND samples of a range of dilutions with DI water were prepared by the plunge-freezing method using the commercial FEI Vitrobot. The detailed steps involve (1) blotting the 1 μml of DND in water to generate a thin liquid film on a holey-carbon coated TEM grid; (2) The grid was then rapidly plunge into a mixture of liquid nitrogen and liquid ethane; (3) The frozen samples were then transferred (in liquid nitrogen) into the cartridge of the TEM specimen auto-loader. The cryogenically frozen DND in water was imaged using a cryo-TEM, Krios (Thermofisher) at 300 kV at ASU. The images were taken using the single-electron-detection camera, K2 (Gatan, Inc), allowing high-quality and high contrast imaging taken at low electron dose (dose rate of 1 electron/pixel/ second and total dose of 30/Å^2.) For each image, 10 subframes of 2 sec exposure time per frame was used (giving a total exposure time of 20 sec). The specimen drift between each frame was corrected and the total 10 frames was averaged to give a final resultant image.

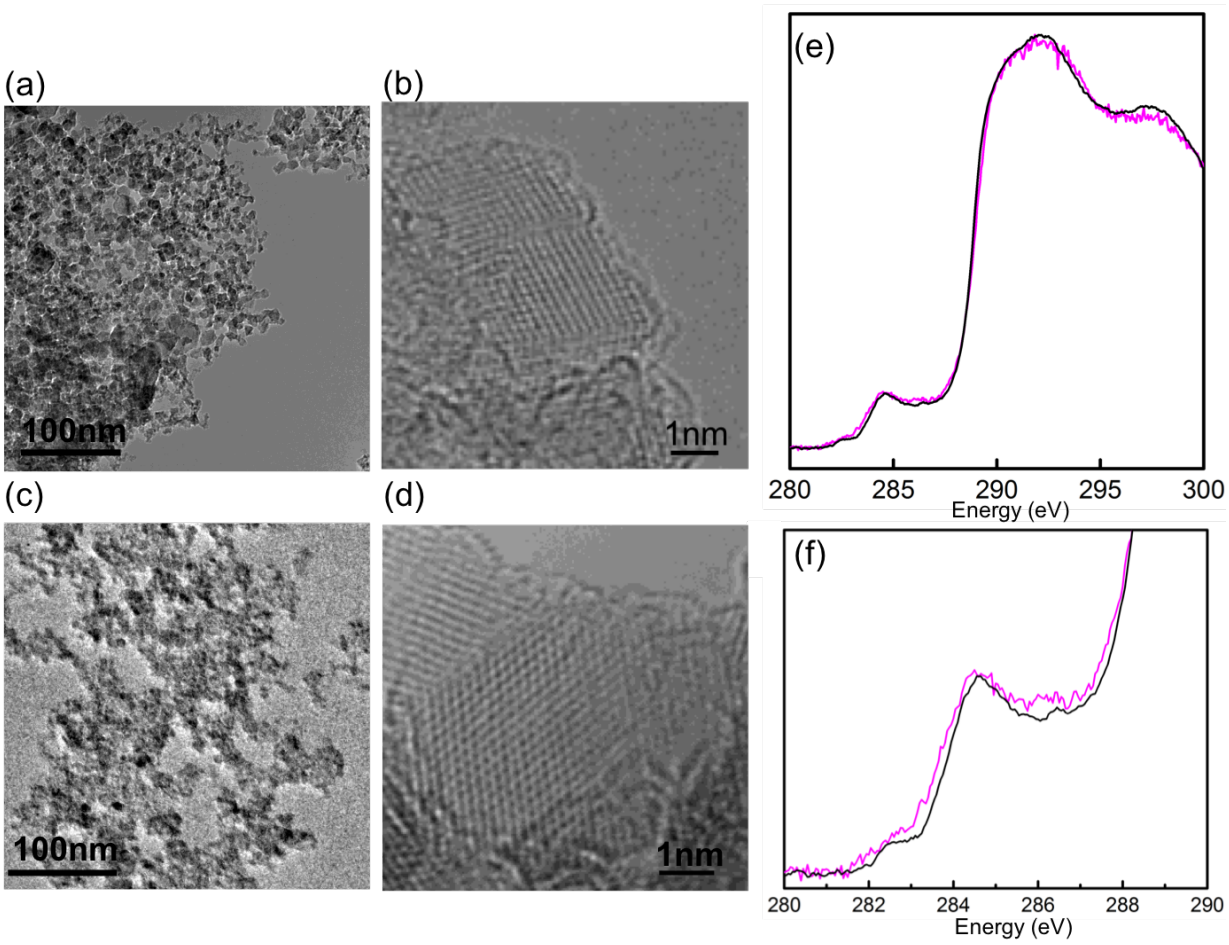

FIG. S2. Atomic and electronic structures of DND particles with surface chemistry rich in C-H and carboxylic group, respectively. (a-b) Bright field and high-resolution TEM images of DND with rich in C-H group and (c-d) those rich in carboxylic group. (e) C K-edge EEL spectra of DND shown in (a-b) (black) and shown in (c-d) (magenta) and (f) the enlarged view of the near edge structure.

D. Atomic and electronic structure of detonation nanodiamond using HRTEM imaging and Electron energy loss spectroscopy

TEM imaging was performed using a monochromated, and spherical- (C_s) aberration-corrected TEM (FEI Company) operated at 80 kV to give a spatial resolution of 1 Å. Electron energy loss spectroscopy was performed at an energy resolution of 0.2 eV by exciting the monochromator to reduce the energy spread of the incident electrons. The TEM specimens of both types of DND particles were prepared using a standard drop-cast method which

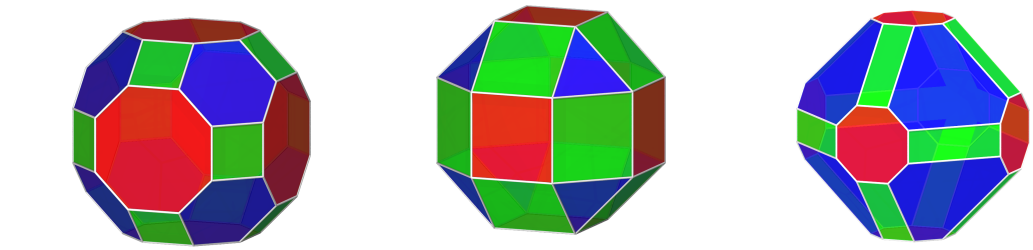

(a) (b) (c)

FIG. S3. Compound shapes including (a) the great rhombicuboctahedron (GRO), (b) the small rhombicuboctahedron (SRO), and (c) the modified truncated octahedron (mTO); each enclosed by {100} (red), {110} (green) and {111} (blue) facets.

involves dropcasting DND suspension onto holey carbon film coated Cu TEM grids and dried in vacuum for 5 minutes. The dried TEM sample (as opposed to the plunge-freezed cryo-TEM samples) show random aggregates of DND particles for both types as shown in S2 (a) and (c). This is typical of dried DND, as this has also been observed consistently in the literature. Common to both types of DND, Fig. S2 (b) and (d) show that the structure of the DND particles composed of diamond cores and fullerenic-like shell(s). Such atomic structures are consistent with the electronic observations using EELS, where the C K-edge (Fig. S2 (e)) shows diamond-like edges with pronounced sp^3 peaks at 289eV. The near edge structure shown in Fig. S2 (f) shows the presence of sp^2 and sp^{2+x} bonds characteristic of fullerene-like surface structure. These characterisations and structural interpretations have been reported previously by both our group and others [1, 5, 6]. Quantitative analysis of the sp^2/sp^3 ratio of the two samples gives 28±3 and 30±3, respectively.

E. Mesoscale simulations of nanodiamond aggregation

In the present study we have used the Simulation of Nanoparticle Assembly using Protoparticles (SNAP) package (under development) to investigate the meso-structure of aggregated faceted polyhedral nanodiamonds. SNAP is a corase-grained molecular dynamics package that has been implemented for cpu (serial, OpenMP and MPI) and gpu (serial and MPI) infrastructures, and replaces groups of surface atoms with like properties with a sparse mesh of interaction points known as *protoparticles* that retain the properties of surfaces cal-

culated using electronic structure methods to improve the speed and efficiency of simulations of >10k entire nanoparticles. Protoparticles interactions occur via a Morse potential which has been parameterized via high level calculations external to SNAP between different combinations of atomistic facets [7–9]. A surface mesh density of 0.2 protoparticles/Å^2 has been used in this study to stop particle overlap which is governed by the range of the repulsive part of the Morse potential. The mesh of protoparticles is held together by a harmonic potential which preserves their initial geometry beyond thermal vibrations. The nanoparticle mass is distributed evenly over the protoparticles and thus represents an approximation in the moment of inertia. The velocity Verlet algorithm is used to integrate the equations of motion using a time step of 3fs and temperature is controlled by simple velocity rescaling. Due to the lack of atomistic bonding in the simulations, there is no definition of a quantitatively accurate temperature. We thus employ a pseudo-temperature for the purpose of quenching and simulations were quenched from a liquid like state to a solid aggregate at a quench rate of 208.3K/ns. More details of the MD methodology can be found in the Supporting Information. SNAP is capable of modeling a mixture of any user-defined shapes, at size ranging from nanometres to microns, parameterised by the user to describe any type of behaviour that can be defined by interaction potential energy wells. We have included three complex polyhedra enclosed by low index {100}, {110} and {111} facets, known to have characteristic positive, near-neutral and negative surface electrostatic potentials, respectively. The facet-dependent surface electrostatic potential has implications and their use[10, 11] and is responsible for the aggregation and self-assembly[1, 12]. The three polyhedral included here are generated *via* the facets using a collection of normal vectors defining each of the nanoparticle's facet planes (akin to a Wulff construction) and include the great rhombicuboctahedron (GRO), which is dominated by positive (100) surface area (Figure S3(a)); the small rhombicuboctahedron (SRO), which is dominated by near-neutral (110) surface area (Figure S3(b)); and the modified truncated octahedron (mTO), which is dominated by negative (111) surface area (Figure S3(c)). The surface enclosed by the intersection of these facet planes is calculated and represented by the generation of an equidistant *protoparticles*. The protoparticles decorating different facets are encoded with different physicochemical properties (as mentioned above) and are the origins of the forces fields describing the interactions between nanoparticles. A surface mesh density of 0.2 protoparticles/Å^2 has been used in this study to stop particle overlap and is governed by the range of the repulsive part of the Morse

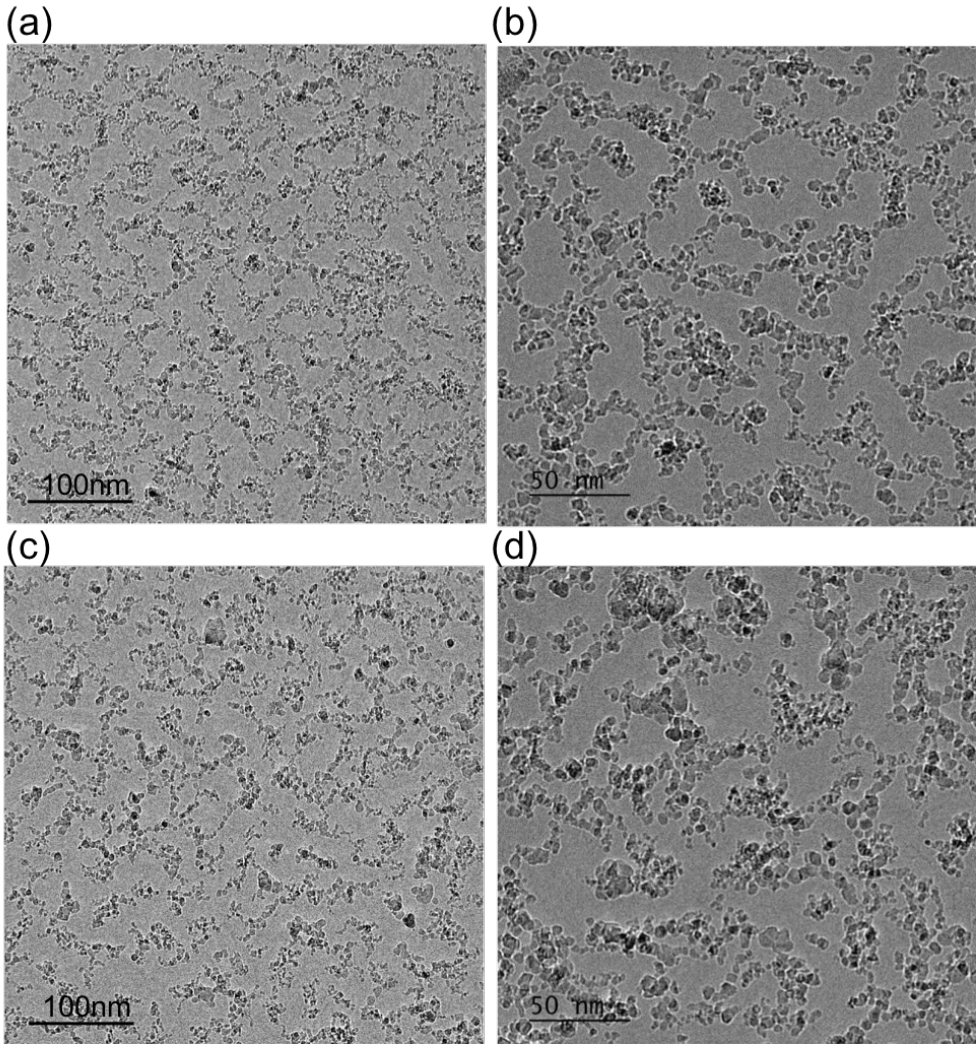

FIG. S4. cryo-TEM images of DND rich in C-H group (a-b) and rich in carboxylic group (c-d) with the same nominal concentration 1w/v%.

potential, parameterised using interactions between different combinations of surface facets reported elsewhere.[7–9]

F. Effect of surface chemistry from the purification process to the DND aggregates

Purified DND generally have complex surface chemistry groups, as shown in Fig.S1. In order to investigate the effect of surface chemistry introduced during the purification process, DND samples with different surface chemistry were imaged. To ensure the fair comparison, same nominal concentration of 1w/v%. It can be seen from Fig. S4 that both types of DND

have very similar aggregate behaviour. Lace-like networks are present for both samples and the enlarged images show the presence of aggregates of rope-like morphology and random clusters. The major difference is that the distributions of the aggregate is less dense in the more diluted sample. Overall, the complex surface chemistry of the purified DND has little impact on the aggregate morphology.

---

[1] L. Y. Chang, E. Ōsawa, and A. S. Barnard, Nanoscale **3**, 958 (2011).

[2] N. Nunn, M. dAmora, N. Prabhakar, A. M. Panich, N. Froumin, M. D. Torelli, I. Vlasov, P. Reineck, B. Gibson, J. M. Rosenholm, S. Giordani, and O. Shenderova, Methods Appl. Fluoresc. **6**, 035010 (2018).

[3] M. Doucet, J. H. Cho, G. Alina, J. Bakker, W. Bouwman, P. Butler, and A. Washington, Zenodo (2018), 10.5281/zenodo.1412041.

[4] B. Hammouda, J. Appl. Crystal. **43**, 716 (2010).

[5] L. Y. Chang, A. S. Barnard, C. Dwyer, C. B. Boothroyd, R. K. Hocking, E. Ōsawa, and J. Nicholls, Nanoscale **8**, 10548 (2016).

[6] J. Raty, G. Galli, C. Bostedt, T. W. van Buuren, and L. J. Terminello, Phys. Rev. Lett. **90**, 037401 (2003).

[7] A. S. Barnard and E. Ōsawa, Nanoscale **6**, 1188 (2014).

[8] A. S. Barnard, J. Mater. Chem. **18**, 4038 (2008).

[9] L. Lai and A. S. Barnard, J. Phys. Chem. Lett. **3**, 896 (2012).

[10] E. Ōsawa, Pure Appl. Chem. **80**, 1365 (2008).

[11] E. Ōsawa, D. Ho, H. Huang, M. V. Korobov, and N. N. Rozhkova, Diamond & Relat. Matter. **18**, 904 (2009).

[12] J. Hees, A. Kriele, and O. A. Williams, Chem. Phys. Lett. **509**, 12 (2011).